Exfoliated/Intercalated Silicate/Hot Styrene Butadiene Rubber Nanocomposites: Structure–Properties Relationship

J. Díez,[1] L. Barral,[1] R. Bellas,[1] J. López,[1] C. Ramírez,[1] A. Rodríguez[2]

[1]*Departamento de Física, E.U.P., Universidad de A Coruña, Avda. 19 de Febrero s/n, 15405 Ferrol, Spain*
[2]*Departamento de Química y Tecnología de Elastómeros, Instituto de Ciencia y Tecnología de Polímeros, CSIC, Juan de la Cierva 3, 28006 Madrid, Spain*

Received 28 February 2011; accepted 19 December 2011
DOI 10.1002/app.36685
Published online 17 February 2012 in Wiley Online Library (wileyonlinelibrary.com).

ABSTRACT: Rubber nanocomposites based on hot styrene-butadiene rubber (SBR) and organophilic layered silicate were prepared via mechanical mixing followed by compression molding. Varying amount of organically modified nanosilicate, 2.5, 5, 10, and 15 parts per hundred of rubber (phr), was added to the SBR matrix to examine the influence of nanosilicate on morphology and structure–property relationships. The morphology of nanocomposites was studied by X-ray diffraction and transmission electron microscopy which reveal that the nanocomposite contained a good dispersion of intercalated/exfoliated layers through the matrix. The interaction between SBR matrix and nanofiller was studied by infrared spectroscopy. No clear evidence for the formation of new components in the rubber was found but infrared spectroscopy denoted evidence for exfoliation. The reinforcing effect of the nanosilicate was determined by mechanical testing and dynamomechanical analysis. The results indicate that the tensile properties and the storage modulus increased with increasing nanofiller loading. This suggests a strong rubber–nanosilicate interaction which is attributed to the exfoliated/intercalated structure. Thermogravimetric analysis revealed that incorporation of organoclay enhances the thermal stability of the nanocomposites. The best thermal stability was observed for nanocomposites containing 5 phr nanosilicate. © 2012 Wiley Periodicals, Inc. J Appl Polym Sci 125: E705–E713, 2012

Key words: rubber; nanocomposites; infrared spectroscopy; structure–properties relations

INTRODUCTION

In the recent years, polymer/clay nanocomposites have emerged as a new class of materials that attracted considerable interest in research because these materials can exhibit potentially superior properties compared with conventional macro and microcomposites.[1] Layered silicates are commonly used as reinforcing filler for preparation of polymer nanocomposites due to their economic competitiveness and wide availability. Due to the nanometric scale of layered silicates with high aspect ratio and high surface area, good reinforcement is possible at very low filler loading (<10%) compared with conventional fillers, which require much larger quantities (>30%).[2] Enhancement of significant properties of nanocomposites is a measure of dispersion of the individual silicate platelets within the polymer matrix. In the literature, two types of morphology are proposed for the layered silicate nanocomposites: intercalated and exfoliated structures.[3] Among them, the completely exfoliated nanocomposites are desired because the exfoliated layers exhibit the greatest reinforcement. The clay used for nanocomposites usually needs to be organically modified, aimed to improve the compatibility of polymer and silicate layers.[4] This is achieved by ion exchange, replacing the original cations present in the clay interlayers by more bulky organic ones, usually alkylammonium cations.

Organoclays have been mainly tested with engineering plastics, but in recent years, rubber/clay nanocomposites have attracted great interest, both in industry and in academy. Styrene-butadiene rubber (SBR) is a commodity elastomer due to its high volume production and its low marked price. SBR is widely employed in the tire industry and for other rubber items. The majority of the studies of SBR nanocomposites have been focused on cold emulsion polymerized SBR, whereas hot SBR have been less investigated. Cold SBR is normally easier to process than hot SBR due to its reduced level of branching, crosslinking, and low molecular weight.[5] However, hot SBRs give better green strength and have exceptional processing characteristics in terms of low mill shrinkage, good dimensional stability, and good extrusion characteristics. Hot SBRs are usable when

Correspondence to: J. Díez (jdiez@udc.es).
Contract grant sponsor: Consellería de Educación, Xunta de Galicia; contract grant numbers: Axudas do Programa de Consolidación Expte. CN2011/008, XUGA 10TMT172009PR.

a low level of dynamic properties and good flow properties are required.[6] Typical applications of hot SBRs include solvent-based adhesives, sealants and coating, or flow modifiers for other elastomers.

The objective of this study is to analyze the effect of nanosilicate content on the material properties of hot styrene-butadiene rubber. The overall properties governed by structure–property relationship are the prime aspect of this study. Physico–mechanical, thermal properties, and morphology are used to evaluate the structure and performance of these composites. The nature of nanosilicate in the SBR matrix was determined by X-ray diffraction (XRD), transmission electron microscopy (TEM), and infrared spectroscopy.

EXPERIMENTAL

Materials

Styrene-butadiene rubber (SBR 1013), a hot emulsion polymerized SBR with an average styrene content of 43.5% and supplied by ISP, was used as the elastomeric matrix. Commercial nanosilicate was purchased from Nanocor, Inc. USA (Nanomer® I.30E). Nanomer® I.30E is a surface-modified montmorillonite with 75%–70% clay and 25–30 wt % octadecylamine (ODA). Sulfur was used as vulcanizing agent in conjunction with a primary organic accelerator (2-mercaptobenzothiazole) and activators (stearic acid and zinc oxide). These reagents (analytical grade) were provided by Aldrich.

SBR nanocomposites preparation

A conventional vulcanization sulfur system was used for compounding. Mixing was performed in an internal mixer Brabender Plasticorder PLE 2000 at a set temperature of 60°C with a rotor speed at 60 rpm. The SBR was masticated for 2 min and then the ingredients were added in the same order given in Table I. Mixing was further continued for 12 min until an equilibrium torque was reached. The formulation of composites expressed as parts per hundred of rubber (phr) is displayed in Table I. Composites with 2.5, 5, 10, and 15 phr nanosilicate were prepared. Moreover, a gum-rubber was prepared without filler. After mixing, the rubber mixtures were left for 24 h at room temperature and then vulcanized at 160°C with 20 MPa pressure using an electrically heated hydraulic press IQAP-LAB PL-15. The optimum cure time (t_{90}) was previously determined by using a moving die rheometer, MDR2000E.

TABLE I
Composition of the SBR/Nanosilicate Composites (in phr)

SBR 1013	100	100	100	100	100
Filler	0	2.5	5	10	15
Estearic acid	1	1	1	1	1
Zinc oxide	5	5	5	5	5
2-Mercaptobenzothiazole	1	1	1	1	1
Sulfur	3	3	3	3	3

Nanocomposites characterization

The cure characteristics were determined at 160°C using a Monsanto Moving Die Rheometer, MDR2000E, at 1.66 Hz frequency and 0.5 arc, as per ISO 6502:1999.

XRD patterns were collected using a Siemens D5000 diffractometer at the wavelength CuK_α = 1.54 Å, a tube voltage at 40 kV, and current of 30 mA. The samples were scanned in step mode by 0.075°/min scan rate in the range $2\theta = 1.15–10°$.

TEM micrographs were taken with a JEOL 1010 microscope, operating at an accelerating voltage of 80 kV. The ultrathin sections of about 100 nm for analysis were microtomed at −120°C using a Power Tome PC-CRX (RMC Products) and directly supported on a copper grid. Furthermore, by using the scale bars supplied in the TEM micrographs, the UTHSCSA Image Tool version 3.00 software was used to measure the aspect ratios of nanosilicate platelets.

Infrared spectra were recorded on a Bruker Vector 22 FTIR spectrophotometer equipped with a Specac Golden Gate™ single reflection ATR system. The spectra were obtained under air atmosphere from at least three sampling points on each specimen, where 64 scans were accumulated at a spectral resolution of 4 cm^{-1} in the wavenumber range of 4000 cm^{-1}–600 cm^{-1}. The contact variability was further minimized by averaging the spectra obtained from each sample.

The crosslink density was estimated by a solvent swelling test. Circular specimens of 10 mm diameter and 3 mm thickness were immersed in toluene during 72 h at 25°C. The weight of the deswollen specimens was determined after removing toluene at 70°C until constant weight was achieved. The crosslink density was determined by the application of Flory-Rehner equation.

The tensile properties (ultimate tensile strength, elongation at break, and modulus at 100% elongation (M100)) of the vulcanizates were measured according to ASTM D638:2003 using dumb-bell-shaped specimens (Type IV). The tear strength was determined according to ISO 34-1:1994 using unnicked angle test pieces. The assays were carried out at room temperature with a crosshead speed of 50 mm/min using an Instron 5566 Universal Test machine.

TABLE II
Curing Characteristics of the SBR/Nanosilicate Composites

Filler (phr)	ts_2 (min)	t_{90} (min)	S_{max} (dNm)	S_{min} (dNm)	CRI (min^{-1})
0	15.96	61.95	6.99	0.37	2.17
2.5	10.62	34.66	8.26	0.41	4.15
5	11.40	35.99	7.79	0.47	4.07
10	10.60	34.57	7.59	0.55	4.17
15	7.64	31.43	8.69	0.68	4.20

Shore A hardness was measured using a Hampden M202 durometer according to ISO 638:2003 test method.

The compression set was assessed according to ISO 3384:1999 at a test temperature of 70°C for 24 h. Standard test specimens of cylindrical shape with 20 mm diameter and 15 mm thickness were used and the percentage of compression employed was 25% of the samples original thickness.

The dynamomechanical analysis was carried out in a Perkin Elmer DMA7 dynamomechanical analyzer using rectangular samples of 7.5 mm × 3 mm × 0.7 mm (length × width × thickness) and extension-film geometry. Testing was performed in the temperature scan mode heating from −70°C to 70°C at a rate of 2°C/min and 1 Hz of frequency.

Thermal degradation measurements were carried out on Perkin Elmer TGA7 thermobalance at a heating rate of 10°C/min under argon atmosphere.

RESULTS AND DISCUSSION

Cure characteristics

Table II shows the cure characteristics of the SBR nanocomposites. Note that both vulcanization times, ts_2 and t_{90}, were sharply reduced in presence of the nanosilicate. It was also found that the cure rate index, CRI, defined as $CRI = 100/(t_{90} - ts_2)$, doubled its value with the filler addition. The maximum torque was also increased in the filled samples.

The general mechanism for the accelerated sulfur-vulcanization is thought to be as follows. First, the accelerators and activators react to generate an active accelerator complex that reacts with sulfur to give an active sulfurating agent. Second, this species reacts preferentially with allylic hydrogen atoms of rubber to form initial crosslinks. As the cure proceeds, these crosslinks are broken down to form mono and disulfidic crosslinks.[7] The organophilic silicate behaves as an accelerant agent for SBR vulcanization. This accelerating effect was attributed to a transition complex formation with amines and sulfur-containing compounds. Nieuwenhuizen et al.[8] have studied the role of zinc accelerator complexes in sulfur-vulcanized systems underlying the action of amines. They refer a mechanism where a nucleophilic attack of an amine on the carbon atom of zinc sulfurating agent yields an amine-dithiocarbamic intermediate. The presence of the curatives inside or at the edges of the silicate layers could generate such complexes. The tethered ODA chain will leave the clay surface in order to participate in the vulcanization intermediate. This occurs either by migrating into the rubber matrix or causing rubber crosslinking inside the galleries.[9]

Morphology

Two complementary techniques used for the characterization of nanocomposites are X-ray diffraction and transmission electron microscopy.

X-ray diffraction patterns of clay reflect the ordered arrangement of silicate layers. The filler (Nanomer® I.30E) diffractogram exhibited a diffraction peak at $2\theta = 4.26°$.[10] The interlayer distance (d), calculated using Bragg's equation from the first order basal reflection, was 2.07 nm. In the SBR nanocomposites, the clay diffraction peak was shifted toward lower angles as a result of an interlayer

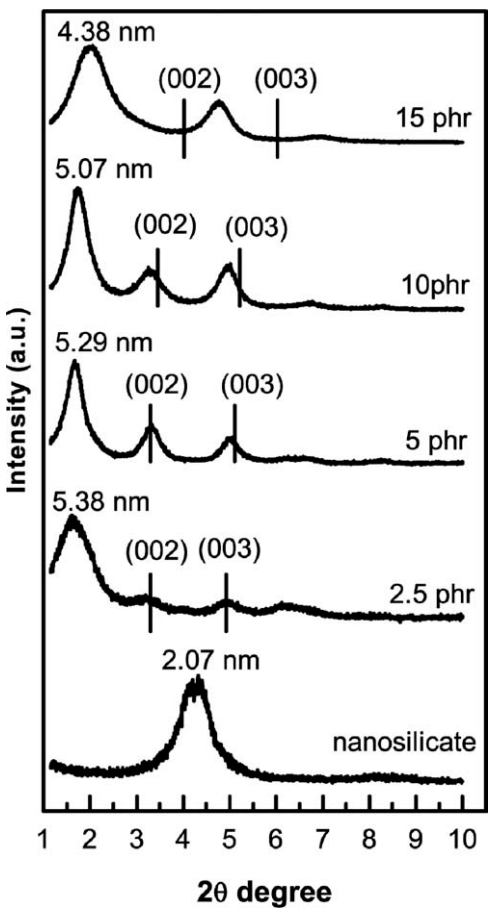

Figure 1 X-ray diffraction patterns for SBR/nanosilicate composites.

spacing increase (Fig. 1). This provides evidence for the penetration of polymer chains into clay layers, giving an intercalated structure.

The extent of intercalation depends on several factors such as the diffusion of elastomer chains within silicate galleries, agglomerate size, and the nature of elastomer itself. Although it is thought to be independent of the filler concentration,[11] the increase in filler led to less intercalation of the rubber into the galleries of the silicate layers, which means smaller interlayer distances.

Additionally, small peaks were observed for the nanocomposites. The origin of these peaks is not so obvious. If the peak is due to secondary or higher order reflections, the parameter n in the Bragg law change, but the distance calculated is the same as the first peak. The calculated positions of the reflections at higher order are indicated by vertical lines in Figure 1. We think that these additional peaks are related on both reflections at higher order and some deintercalation phenomena.[12] It is believed that the amine functionality of octadecylamine can be removed (extracted) from the interlayer to participate in the zinc-accelerator complexes. Thus, the clay layers collapse and the interlayer distance is reduced.[9,13]

It is of interest to check how the TEM technique can contribute to clarify the dispersion of the filler in the SBR matrix and the presence of structural heterogeneities. Figure 2 shows characteristic TEM microphotographs of the nanocomposite with 15 phr nanosilicate at various magnifications. The darker phase represents the filler, whereas the clearer phase is the rubber matrix. The aspect ratios of nanosilicate platelets were calculated by measuring length and thickness of the dark lines in TEM micrographs at different magnifications. The nanosilicate layers are uniformly dispersed as platelets of around 136 ± 38 nm length and 9 ± 4 nm thickness. The clay layers show some orientation and we assumed that alignment is governed by the degree of shear during mixing and compression molding. TEM images confirm the existence of exfoliated layers as well as some large silicate aggregates.

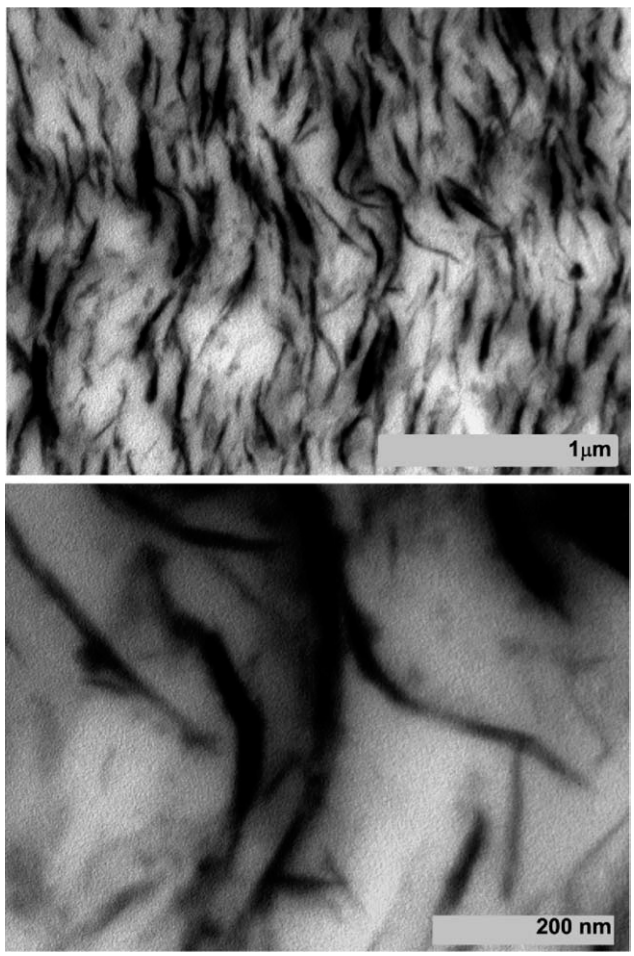

Figure 2 TEM micrographs of SBR composite with 15 phr nanosilicate at various magnifications (indicated).

Infrared spectroscopy

Figure 3(a) shows the infrared spectra of the nanosilicate filler in powdered form in the region 4000 cm^{-1} to 800 cm^{-1}. The most typical band for the montmorillonite corresponds to a broad feature between 1100 cm^{-1} and 1000 cm^{-1} attributed to the vibrations of different Si–O bonds in the clay structure.[14] Other bands are located at 1467 cm^{-1} (assigned to the ammonium salt), at 2923 cm^{-1} and 2849 cm^{-1} (due to the C—H asymmetric and symmetric stretching vibrations of octadecylamine, respectively) and at 3627 cm^{-1} (owing to the —OH stretching vibration of montmorillonite).

The Si–O region of the spectrum is rather complex with several overlapping spectral features. One silicate layer contains two kinds (in what concerns the orientation) of Si–O bonds. The first one involves the basal oxygens of the silicon–oxygen tetrahedra and has their transition moment lying in the plane of the layer; these vibrational modes are designated "in-plane." The second one corresponds to the silicon–oxygen bonds directed toward the octahedrally coordinated aluminum ions and has their transition moment perpendicular to the layer; these modes are designated "out-of-plane."[15] In the literature, four overlapping bands are identified in the Si–O region: three in-plane ($\sim$ 1120 cm^{-1}, $\sim$ 1048 cm^{-1}, and $\sim$ 1025 cm^{-1}) and one out-of-plane ($\sim$ 1080 cm^{-1}), designated as peak I, III, IV, and II, respectively.[16] If the clay layers are agglomerated into stacks (tactoids) and particles thereof, the absorption bands appear as a broad peak as a result of in-plane and out-of-plane contributions.[17] Montmorillonites are natural materials and do not possess a perfect

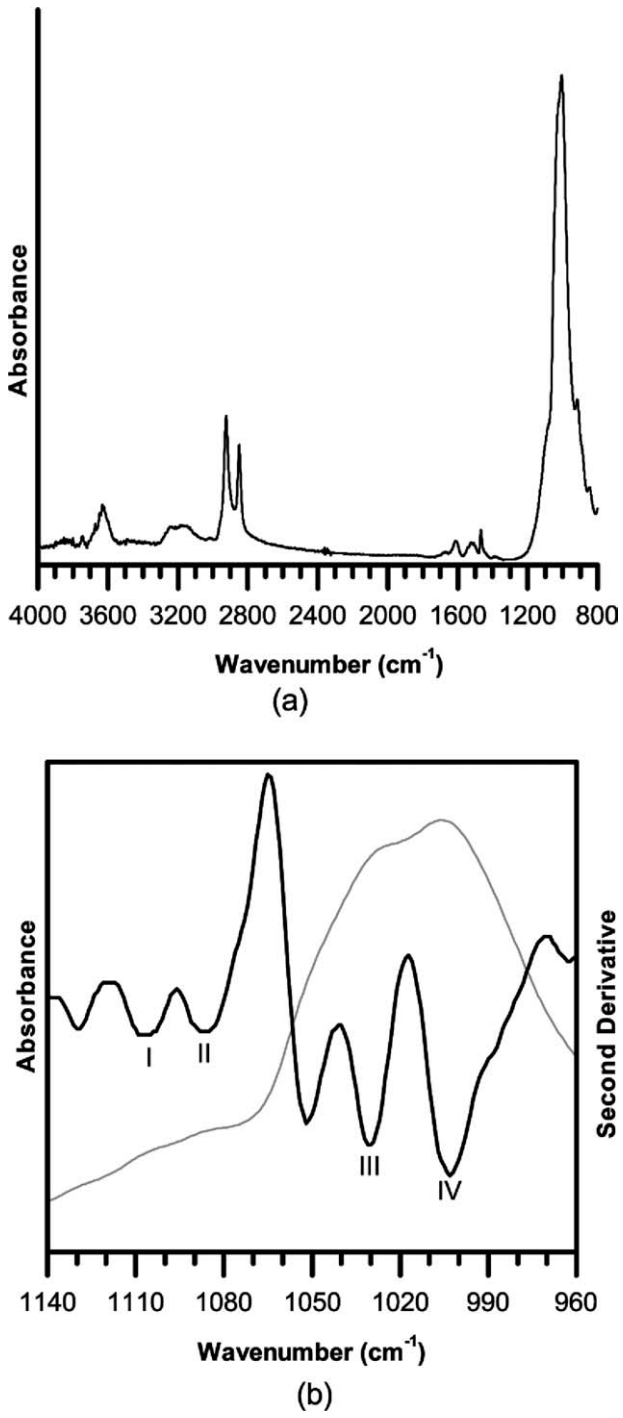

Figure 3 ATR-FTIR spectra of neat nanosilicate Nanomer® I.30E: (a) absorbance spectrum and (b) second-order derivative spectrum.

crystalline structure but rather a distribution of somewhat imperfect structures. As a result, the peak's appearance for the nanoclay used corresponds to the initial tactoids [Fig. 3(b)]. Unfortunately, a rigorous peak fitting was difficult to achieve, owing to the complexity of the spectra, but derivative routine may be useful in improving spectra interpretation. The second derivative procedure, applied to the clay spectra in the spectral range between 1140 cm^{-1} and 960 cm^{-1}, indicated the presence of five Si–O peaks located at 1107 cm^{-1}, 1030 cm^{-1}, and 1003 cm^{-1} (peaks I, III, and IV), 1086 cm^{-1} (peak II), and 1052 cm^{-1}. The later peak was observed previously in organically modified montmorillonites.[18]

The infrared spectra of SBR and its composites after normalization of the spectra on the styrene peak at 697 cm^{-1} are shown in Figure 4. The spectra are relatively heterogeneous and contain information both of the components of vulcanized SBR as well the clay filler. Compounding ingredients exhibit their corresponding absorption band as well. For instance, the band at 1539 cm^{-1} is attributed to the asymmetric —C=O band of Zn-stearate, originating from the reaction of zinc oxide with stearic acid during the vulcanization process.

The broad bands in the Si–O stretching region increase in relative intensity with increasing content of nanosilicate. No clear evidence for the formation of new components in the rubber was found, in agreement with our previous work with cold SBRs.[10]

Infrared spectra have been widely used to characterize the polymer-clay nanocomposites in order to evidence the presence of all the constituents, but more recent studies are using this technique to asses the delamination of clays. The main object of this experiment was to study the behavior of the clay peak. For this, the clay spectrum is generated by subtracting the spectrum of SBR from the spectrum of nanocomposites; the polymer peaks are eliminated and a clean spectrum is obtained for further analysis (Fig. 5).

A significant variation in the profile of the Si–O stretching region, in comparison with the spectra of pure organoclay, can be observed. In nanocomposites, well-splinted peaks can be visualized, which are corresponding to in-plane and out-of-plane Si–O modes. The main characteristic is that the out-of-plane

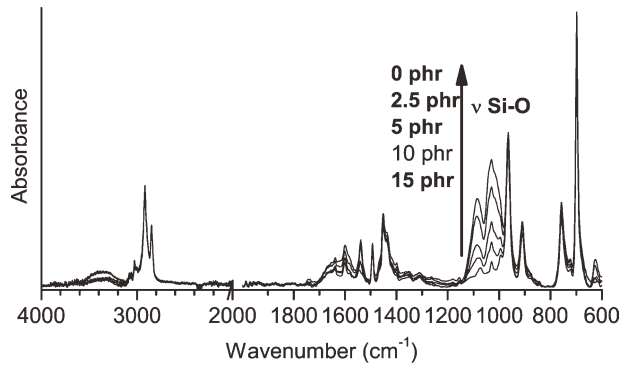

Figure 4 Infrared spectra of SBR nanocomposites normalized at 697 cm^{-1}, with increasing nanosilicate content, shown by arrow in Si–O stretching region (scale change at 2000 cm^{-1}).

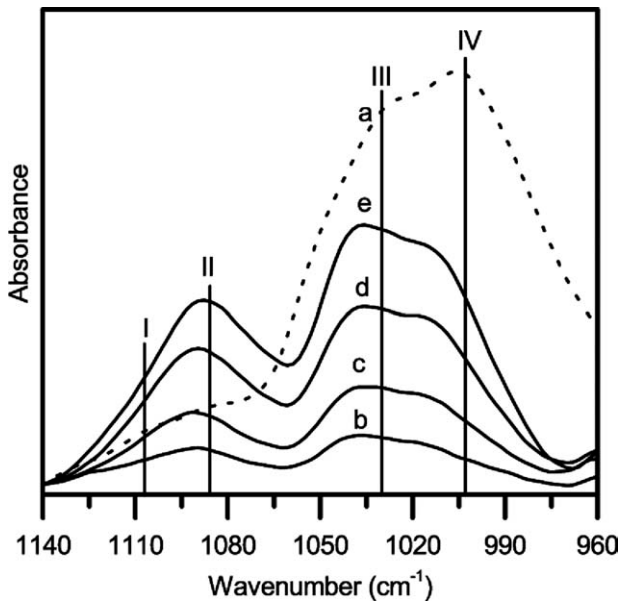

Figure 5 Infrared spectra from 1140 cm^{-1} to 960 cm^{-1} of neat nanosilicate (a) and the subtracted spectra of the nanosilicate in the SBR nanocomposites with 2.5 phr (b), 5 phr (c), 10 phr (d), and 15 phr (e) filler loadings.

vibration is clearly resolved when the clay is in the rubber matrix. Peak III and IV are quite strong in nanocomposites, whereas peak I cannot be detected in the absorbance spectra. A general shift toward higher frequencies of the Si–O modes, compared with neat organoclay, is evident. The spectra appearance for the clay in nanocomposites is almost identical to the spectrum of a completely delaminated montmorillonite in water described by Ijdo et al.[14] This behavior indicates evidence for clay exfoliation.

Because the overall intensity variation in Figure 5 is dependent on the clay content, some attempts to quantify the peak height were done and the peak ratios were calculated. For this, the second derivative curves were explored and the peak height was quantified in the second-derivative spectra as described by Cole.[19] Peak heights were calculated with respect to the maximum value near 1060 cm^{-1}. The variation of peak ratios with clay loading is plotted in Figure 6. The ratio of peak II to peak IV tends to decrease with clay loading, whereas the ratios of peak III to IV and the ratio of peak II to III show no clear trend with the filler dose. Although the ratio of peak II to peak III increases with clay loading up to 10 phr and above that the ratio start to decrease, the intensity of peak III to IV show the opposite trend. Further work is required to interpret this behavior.

Crosslink density

Since crosslinked rubbers are insoluble in organic solvents, they undergo swelling instead. As the solvent diffuses into the rubber and the material begins to swell, the polymer chains are expanded as if they were exposed to an external three-dimensional force. The two effects—the swelling effect of the solvent and the resisting force of the polymer network—tend to balance out at equilibrium degree of swelling. The final extent of swelling depends on the degree to which the network is crosslinked.

The volume fraction of rubber in the swollen network at equilibrium, Φ_r, is given by the equation of Ellis and Welding[20]:

$$\phi_r = \frac{(D - fw)\rho_r^{-1}}{(D - fw)\rho_r^{-1} + A_s\rho_s^{-1}} \quad (1)$$

where D is the deswollen weight, f is the volume fraction of filler, w is the initial weight of the polymer, ρ_r and ρ_s are the densities of the rubber and the solvent, respectively, and A_s is the weight of the absorbed solvent.

The average molecular mass between crosslinks, M_c, can be calculated by using the Flory-Rehner equation,[21] which relates M_c to the measured volume rubber fraction in the swollen state:

$$M_c = [-\rho_r V_s (\phi_r^{1/3} - \phi_r/2)]/[\ln(1 - \phi_r) + \phi_r + \chi\phi_r^2] \quad (2)$$

where V_s is the molar volume of toluene and χ is the Flory-Huggins polymer–solvent interaction term. χ can be calculated using the following expression:

$$\chi = \beta + \frac{V_s}{RT}(\delta_s - \delta_r)^2 \quad (3)$$

where δ_s is the solubility parameter of the solvent, β is the entropic contribution which value is taken as

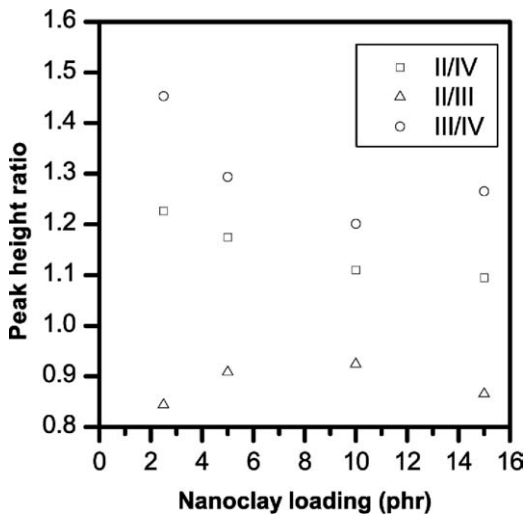

Figure 6 Variation of peak height ratios as a function of clay loading.

TABLE III
Crosslink Density and Mechanical Properties of SBR/Nanosilicate Composites

Filler (phr)	Crosslink density (mol m^{-3})	Elongation at break (%)	Tensile strength (MPa)	M100 (MPa)	Hardness shore A	Tear strength (kN/m)	Compression set (%)
0	168 ± 6	292 ± 14	1.91 ± 0.09	0.88 ± 0.01	45.9 ± 0.9	10.6 ± 1.2	7.6 ± 0.3
2.5	155 ± 8	336 ± 12	2.60 ± 0.09	1.06 ± 0.01	50.3 ± 0.3	13.5 ± 0.6	10.2 ± 0.2
5	165 ± 5	364 ± 16	2.82 ± 0.14	1.12 ± 0.01	51.1 ± 0.6	13.2 ± 0.6	14.6 ± 0.1
10	137 ± 2	383 ± 45	3.49 ± 0.45	1.45 ± 0.03	55.2 ± 1.5	16.3 ± 3.6	19.0 ± 1.1
15	134 ± 2	437 ± 23	5.06 ± 0.28	2.01 ± 0.04	61.1 ± 1.4	25.3 ± 2.9	23.9 ± 1.4

0.34,[22] R is the universal gas constant, T is the absolute temperature, and δ_r is the solubility parameter of the rubber. δ_r values was estimated from functional groups contribution using the Hoftyzer and Van Krevelen method.[23] The interaction parameter (χ), calculated using eq. (3), was 0.3420.

Using the M_c values, crosslink density (ν) can be calculated as follows:

$$\nu = \rho_r / M_c \tag{4}$$

The nanosilicate incorporation led to a decrease in crosslink density values (Table III). This behavior was unusual but we observed a similar trend in the crosslink density of cold SBR reinforced with organoclay.[24] During vulcanization, sulfur free radicals are formed and they attack polymer chains to form macroradicals. These macroradicals react with each other and form crosslinks. If a polymer chain intercalates between two silicate layers, it can hardly find another chain to react with; i.e., silicate layers behave like obstacles that prevent crosslink reactions and therefore, the crosslink density decreases.[25] On the other hand, the partial absorption of the curatives on the filler surface cannot be ruled out.

Mechanical properties

A feature of polymer/clay nanocomposites is their remarkably improved mechanical properties. There are several factors that influence the tensile properties of polymer nanocomposites, such as the interaction between the clay and polymer matrix, the method of preparation, and the filler loading. It has been demonstrated that the complete dispersion of clay nanolayers in a polymer optimizes the number of available reinforcing elements carrying an applied load and deflecting cracks.[26] Interaction between the clay platelets having large surface area and the rubber chains facilitates stress transfer to reinforcement phase, resulting in improved tensile properties.

The effect of nanosilicate on the mechanical properties of SBR was analyzed, and the results are summarized in Table III. SBR nanocomposites showed a remarkable enhancement in ultimate tensile strength, which increased with increase in nanosilicate content. An increment of 265% on the tensile strength was observed at 15 phr filler loading in comparison with unfilled SBR. This improvement can be explained by the dispersion of the nanosilicate in the SBR matrix.[4] The elongation at break was also improved and increased almost linearly with the filler content. However, the increase in elongation at break with rising nanofiller content is not general feature for this kind of nanocomposites. Cataldo reported a gradual reduction in elongation at break values in nanoclay filled rubber, consequence of the stiffening effect exerted by the nanoclay added.[27] The results obtained may be explained by the intercalated/exfoliated microstructure, which allows silicate layers orient along the direction of stress and contribute to increase tensile strength and elongation at break.[5,28]

The reinforcing effect was estimated according to the values of the modulus at 100% elongation, M100, which is a parameter commonly used in rubber technology. Note that M100 increased with filler loading linearly and the maximum enhancement was observed at 15 phr nanosilicate.

The effect of filler addition on tear strength is also summarized in Table III. It was observed that the tear strength increased with nanosilicate loading. A value of 25.3 kN/m was obtained for the nanocomposite with 15 phr filler that means an improvement of 239% over unfilled rubber. This behavior can be explained by the dispersion of nanosilicate at nanometre level and the high interfacial action between the layers and the rubber. The dispersed silicate layers may divert the tear path, which in turn impart high tear strength to nanocomposites.[28]

The hardness of the SBR nanocomposites was also found to increase with increasing filler. Shore A passed from a value of 45.9 in the unfilled rubber to 61.1 at 15 phr nanosilicate loading. This enhancement was related to a higher stiffness of the nanocomposites.

The ability for the SBR nanocomposites to recover after having been under constant deflection was evaluated. Compression set values increased with the increment of filler. The lower the compression set the better is the elastic recovery of the nanocomposite. The worse elastic recovery observed could be

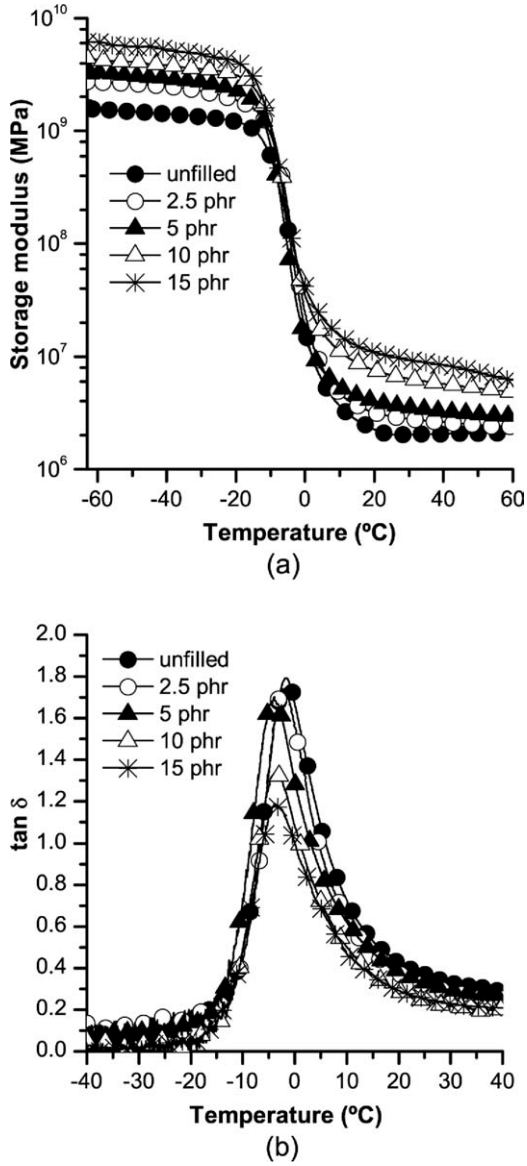

Figure 7 Storage modulus (a) and tan δ (b) as a function of the temperature for pristine SBR and SBR nanocomposites.

due to the energy dissipation contributed by the chain slipping along the nanosilicate surface.[29]

The changes of hot SBR properties by adding clay showed a similar trend to those observed for cold SBR[24] and were in agreement with the morphology observations.

Dynamomechanical analysis

Dynamic mechanical properties are measured to investigate the degree of filler–matrix interaction of SBR nanocomposites. The dynamic storage modulus of pristine SBR and its nanocomposites versus temperature is shown in Figure 7(a). The modulus of SBR nanocomposites is higher than that of unfilled SBR, which reflects the strong confinement of nanodispersed silicate layers on the rubber chains. The effectiveness of filler on the moduli of the composites can be represented by a coefficient C such as follows[30]:

$$C = \frac{(E_g/E_r)_c}{(E_g/E_r)_r} \tag{5}$$

where E_g and E_r are the storage modulus values in the glassy and rubbery region, respectively, and the subscripts "c" and "r" denote the composite and gum-rubber. The higher value of the constant C, the lower the effectiveness of the filler.[30] The measured values at −60°C and 25°C were employed as E_g and E_r, respectively. The C values obtained for the nanocomposites are given in Table IV. The lowest value has been obtained for 15 phr nanosilicate loading.

The variation of loss tangent (tan δ) with temperature is shown in Figure 7(b). The temperature corresponding to tan δ maximum was taken as the glass transition temperature (T_g). Figure 7(b) shows that the addition of nanosilicate results in a slight reduction of T_g values, owing to the restriction of polymer segmental mobility and decrease in volume fraction of the rubber. The intensity of tan δ peak at the glass transition temperature decreases with filler loading (Table IV). This behavior suggests that there are molecular relaxations in the composites which are not present in the pristine rubber. According to Schon and Gronski,[31] the decrease in intensity of the tan δ peak can be used as an indication of higher degree of intercalation/exfoliation. When a greater amount of polymer is between the clay layers, the amount of polymer in the amorphous matrix is reduced.

Thermal stability

The results of thermal analysis are summarized in Table V. The characteristic parameters selected were the maximum degradation temperature (DTG_{max}), which is the highest thermal degradation rate temperature, the temperature at which 50% degradation occurs (T_{50}) and the onset temperature, which is the initial weight loss temperature. It is observed that the thermal stability was improved by nanosilicate addition. The nanocomposites DTG_{max} showed a drastic shift toward higher temperatures, with a

TABLE IV
Filler–Matrix Interaction and Reinforcing Efficiency of SBR/Nanosilicate Composites

Filler (phr)	C	Tan δ_{max}
0		1.79
2.5	1.07	1.74
5	1.06	1.66
10	0.59	1.33
15	0.45	1.25

TABLE V
TG Data for SBR/Nanosilicate Composites

Filler (phr)	DTG (°C)	T_{50} (°C)	Onset (°C)	Residue (%)
0	426 ± 1	438 ± 2	402 ± 3	4.8 ± 0.6
2.5	434 ± 2	444 ± 2	407 ± 1	6.4 ± 0.2
5	471 ± 2	455 ± 1	409 ± 3	7.9 ± 0.2
10	476 ± 5	456 ± 1	404 ± 2	10.5 ± 0.3
15	470 ± 1	452 ± 1	397 ± 2	12.9 ± 0.2

stabilization as high as 45°C at 5 phr nanosilicate. Also, T_{50} showed a noticeably increase. The improvement was much higher than that observed in cold SBR with similar amounts of filler.[24]

The best thermal stability was achieved for nanocomposites containing 5 phr nanosilicate. Above this filler loading, the thermal stability remains unchanged. The better thermal stability of nanocomposites can be attributed to the nanoscale montmorillonite layers preventing out-diffusion of the volatile decomposition products.[32] However, the alkylammonium cations in the organoclay could undergo decomposition which could explain the decrease in the onset of degradation value observed in the nanocomposite with 15 phr nanosilicate.

The residual material of pure SBR was 4.8%, which was the residue of ingredients of the SBR vulcanizates, such as ZnO. The amount of residue increased with filler loading due to that during organoclay degradation only water and octadecylammonium ions are evolved.[24]

CONCLUSIONS

Rubber nanocomposites based on hot SBR have been studied varying the nanoclay loading up to 15 phr. The vulcanization rate of the nanocomposites was found to be sensibly higher than the unfilled SBR. This effect was attributed to the ammonium groups present in the nanosilicate structure that acts accelerating the vulcanization reaction. The X-ray diffraction studies revealed the formation of an intercalated nanocomposite. TEM microphotographs showed the presence of both exfoliated and aggregated structures in the SBR matrix. Infrared spectroscopy indicated evidence for exfoliation.

Most mechanical properties were significantly improved by the addition of nanosilicate even at low loading (5 phr). The most important factor that determines the improvement of properties in rubber by nanoclay incorporation is the distribution in the rubber matrix. This enhancement was explained by the intercalated and exfoliated structures, which cause several fold increase in nanosilicate surface area enhancing the rubber matrix interaction. Dynamic storage moduli increase with increasing nanosilicate loading, and tan δ_{max} values decrease with increased filler loading, owing to a restriction of polymer segmental mobility. Nanosilicate addition also improved thermal stability even at low filler loadings. The overall optimal properties were achieved with 5 phr nanosilicate loading without any detrimental effect.

References

1. Barick, A. K.; Tripathy, D. K. Polym Eng Sci 2010, 50, 5112.
2. Teh, P. L.; Mohd Ishak, Z. A.; Hashim, A. S.; Karger-Kocsis, J.; Ishiaku, U. S. J Appl Polym Sci 2004, 94, 2438.
3. Ray, S. S.; Okamoto, M. Prog Polym Sci 2003, 28, 1539.
4. Mousa, A.; Karger-Kocsis, J. Macromol Mater Eng 2001, 286, 260.
5. Minari, R. J.; Gugliotta, L. M.; Vega, J. R.; Meira, G. R. Ind Eng Chem Res 2006, 45, 245.
6. School, R. In Rubber Technology: Compounding and Testing for Performance; Dick, J. S., Ed.; Hanser Publishers: Munich, 2001; Chapter 6.
7. Diez, J.; Bellas, R.; López, J.; Santoro, G.; Marco, C.; Ellis, G. J Polym Res 2010, 17, 99.
8. Nieuwenhuizen, P. J.; Ehlers, A. W.; Haasnoot, J. G. J Am Chem Soc 1999, 121, 163.
9. Gatos, K. G.; Karger-Kocsis, J. Polymer 2005, 46, 3069.
10. Diez, J.; Barral, L.; Bellas, R.; Bouza, R.; López, J.; Marco, C.; Ellis, G. Polym Eng Sci 2011, 51, 1720.
11. Vu, Y. T.; Mark, J. E.; Pham, L. Y. H.; Engelhardt, M. J Appl Polym Sci 2001, 82, 1391.
12. Ma, Y.; Wu, Y.-P.; Zhang, L.-Q.; Li, Q.-F. J Appl Polym Sci 2008, 109, 1925.
13. Varghese, S.; Karger-Kocsis, J.; Gatos, K. G. Polymer 2003, 44, 3977.
14. Ijdo, W. L.; Kemmetz, S.; Benderly, D. Polym Eng Sci 2006, 46, 1031.
15. Yan, L.; Roth, C. B.; Low, P. F. Langmuir 1996, 12, 4421.
16. Cole, K. C. Macromolecules 2008, 41, 834.
17. Ianchiş, R.; Donescu, D.; Corobea, M. C.; Petcu, C.; Ghiurea, M.; Serban, S.; Radovici, C. Colloid Polym Sci 2010, 288, 1215.
18. Tzavalas, S.; Gregoriou, V. G. Vib Spectrosc 2009, 51, 39.
19. Cole, K. C. Appl Spectrosc 2009, 63, 1343.
20. Jacob, A.; Kurian, P.; Aprem, A. S. J Appl Polym Sci 2008, 108, 2623.
21. Flory, P. J. Principles of Polymer Chemistry; Cornell University Press, Ithaca: New York, 1992.
22. Marzocca, A. J. Eur Polym J 2007, 43, 2682.
23. Van Krevelen, D. W. Properties of Polymers: Their Correlation with Chemical Structure, Their Numerical Estimation and Prediction from Additive Group Contributions; Elsevier Science: Amsterdam, 1990.
24. Diez, J.; Bellas, R.; Ramírez, C.; Rodríguez, A. J Appl Polym Sci 2010, 118, 566.
25. Khanlari, S.; Kokabi, M. J Appl Polym Sci 2011, 119, 855.
26. LeBaron, P. C.; Wang, Z.; Pinnavaia, T. J. Appl Clay Sci 1999, 15, 11.
27. Cataldo, F. Macromol Symp 2007, 247, 67.
28. Madhusoodanan, K. N.; Varghese, S. J Appl Polym Sci 2006, 102, 2537.
29. Park, K. W.; Kim, G. H.; Chowdhury, S. R. Polym Eng Sci 2008, 48, 1183.
30. Praveen, S.; Chattopadhyay, P. K.; Jayendran, S.; Chakraborty, B. C.; Chattopadhyay, S. Polym Int 2010, 59, 187.
31. Schon, F.; Gronski, W. KGK-Kautsch Gummi Kunstst 2003, 56, 166.
32. Chen, G.; Liu, S.; Chen, S.; Qi, Z. Macromol Chem Phys 2001, 202, 1189.